THÈSE DE DOCTORAT
DE SORBONNE UNIVERSITÉ

Spécialité : Physique
École doctorale n°564: Physique en Île-de-France

réalisée

au Laboratoire Kastler Brossel

sous la direction de Pierre-François Cohadon

présentée par

Pierre-Edouard Jacquet

pour obtenir le grade de :

DOCTEUR DE SORBONNE UNIVERSITÉ

Sujet de la thèse :

Progress towards cryogenic squeezed light optomechanics

soutenue le ????? 2025

devant le jury composé de :

M. Mr.	Rapporteur
M. Mr.	Rapporteur
M. Mr.	Examinateur
Mme.coucou	Examinatrice
Mme.salut	Présidente du Jury
M. aurevoir	Directeur de thèse

Remerciements

Merci bien

Contents

I Introduction 3

I.1 Historical background 3

I.2 State of the art 3

I.3 Relevance of this work 3

II Theory:

Background 5

II.1 Quantum Optics Concepts 7

II.1.1 Quantum Description of Light 7

II.1.2 Optical Field Modulations 13

II.1.3 Quantum Noise and Uncertainty 15

II.1.4 Sideband Representation 15

II.2 Optical Cavities: Basics 15

II.2.1 Cavity types and Resonance Conditions 15

II.2.2 Spatial and Longitudinal Modes 15

II.2.3 Quantum Langevin Equations 15

II.3 Optical Cavities: Three Mirror Cavities 16

II.3.1 16

II.4 Cavity Optomechanics 16

II.4.1 Radiation Pressure Coupling 16

II.4.2 Quantum Langevin Equations 16

II.4.3 Mechanical Resonators 16

II.4.4 Noise spectra 16

II.4.5 Three Mirror Cavities as Novel Optomechanical Systems 16

II.5 Squeezed Light Theory 16

II.5.1 Single-mode Squeezing 16

II.5.2 Noise Spectra 16

II.5.3 Frequency-dependent Squeezing and its use 16

II.6 Numerical Methods and Simulations 16

III Experimental Methods **17**

III.1 Optical Locking Techniques with PyRPL 18

III.1.1 Proportion-Integral (PI) Controllers 18

III.1.2 Temperature Locks 19

III.1.3 Optical paths Locks 20

III.1.4 Side of Fringe Locks 20

III.1.5 Pound-Drever-Hall Locks 20

III.1.6 Offset frequency Locks 22

III.1.7 Coherent Sideband Locks 22

III.1.8 PyRPL Control Implementation 22

III.2 Optical Cavities and Squeezed Light Generation 22

III.2.1 Cavity Types and Alignement Procedures 22

III.2.2 Bowtie-type Optical Parametric Oscillator (OPO) 22

III.2.3 Phase Matching and Nonlinear Crystals 22

III.2.4 Filter Cavities for Squeezing Rotation 22

III.3 Quadrature Measurement Techniques 22
    III.3.1 Direct Detection with Photodiodes 22
    III.3.2 Balanced Homodyne Detection 22
    III.3.3 Local Oscillator Design and Control 22

IV Experiments:

Optomechanical Three-Mirror Cavity Systems 23

IV.1 System Description and Setup 24
    IV.1.1 Cavity Geometry and CAD Models 24
    IV.1.2 Laser Source and Optical Layout 24
    IV.1.3 Alignment Procedures 24
IV.2 Middle Mirror as Mechanical Resonator 24
    IV.2.1 Plane Membranes: Design and Characterization 24
    IV.2.2 Phononic Crystals: Dahlia Pattern 24
    IV.2.3 Fabrication and Performance Metrics 24
IV.3 Experimental Characterization 24
    IV.3.1 Cavity Mode Scanning and Modematching 24
    IV.3.2 Locking Techniques and Stability 24
    IV.3.3 Ringdown Measurements and Q-factor Analysis 24
IV.4 Data Acquisition and Analysis 24
    IV.4.1 Measurement Setup and Instrumentation 24
    IV.4.2 Spectral Acquisition and Processing 24
    IV.4.3 Feedback Control Implementation 24
IV.5 Introduction to Experimental Methods 24
IV.6 Design of an Optomechanical Fibered Cavity 24
    IV.6.1 Design considerations 24

V Experiments: Frequency Dependent Squeezing 25

V.1 OPO Resonance and Locking 26
  V.1.1 Resonance Conditions and Sweeps 26
  V.1.2 Lock Acquisition and Optimization 26
  V.1.3 Stability Characterization 26
V.2 Quadrature Spectral Analysis 26
  V.2.1 Detection of Squeezing and Anti-squeezing 26
  V.2.2 Spectral Variation with Frequency 26
  V.2.3 Optimal Quadrature Conditions 26
V.3 Filter Cavity Concept 26
  V.3.1 Virgo Filter Cavity 26
  V.3.2 Thermal effects in bichromatic locks 26
Appendix: PDH Derivation 29

Chapter I

Introduction

Contents

I.1 Historical background 3
I.2 State of the art 3
I.3 Relevance of this work 3

I.1 Historical background

I.2 State of the art

I.3 Relevance of this work

Chapter II

Theory: Background

This chapter will cover the elementary concepts required to describe an membrane based optomechanical system in a quantum regime. We will first recall basics on optical field quantization as well describing coherent and squeezed light field, to then turn to the more specific frequency dependent squeezed light field. Secondly, we will cover the mathematical description of a mechanical resonator interacting with a generic coherent optical field, highlighting the differences with the seminal optomechanical system of a mirror on a spring. Finally, we will derive the equations of motions of a membrane based optomechanical system with frequency dependent squeezed optical fields.

Contents

II.1 Quantum Optics Concepts 7
  II.1.1 Quantum Description of Light 7
  II.1.2 Optical Field Modulations 13
  II.1.3 Quantum Noise and Uncertainty 15
  II.1.4 Sideband Representation 15
II.2 Optical Cavities: Basics 15
  II.2.1 Cavity types and Resonance Conditions 15
  II.2.2 Spatial and Longitudinal Modes 15
  II.2.3 Quantum Langevin Equations 15
II.3 Optical Cavities: Three Mirror Cavities 16
  II.3.1 16
II.4 Cavity Optomechanics 16
  II.4.1 Radiation Pressure Coupling 16
  II.4.2 Quantum Langevin Equations 16
  II.4.3 Mechanical Resonators 16
  II.4.4 Noise spectra 16
  II.4.5 Three Mirror Cavities as Novel Optomechanical Systems 16
II.5 Squeezed Light Theory 16
  II.5.1 Single-mode Squeezing 16

II.5.2 Noise Spectra 16
II.5.3 Frequency-dependent Squeezing and its use 16
II.6 Numerical Methods and Simulations 16

II.1 Quantum Optics Concepts

II.1.1 Quantum Description of Light

We introduce briefly field quantization concepts needed to describe monochromatic field propagation and measurements.

Quantised Electromagnetic Field

We consider the quantised electromagnetic field in volume V. The electric field operator can be expressed in the Heisenberg picture as:

$$\hat{\mathbf{E}}(\mathbf{r},t) = i\sum_{\ell} \mathcal{E}_l \left[\hat{a}_\ell \mathbf{f}_\ell(\mathbf{r}) e^{-i\omega_\ell t} - \hat{a}_\ell^\dagger \mathbf{f}_\ell^*(\mathbf{r}) e^{i\omega_\ell t}\right] \tag{II.1}$$

where $\mathcal{E}_l = \sqrt{\frac{\hbar\omega_l}{2\varepsilon_0 V}}$ is the field per photon in mode ℓ with $\hbar$ the reduced Planck constant, ω_ℓ the angular frequency of mode ℓ and ε_0 the vacuum permittivity, $\mathbf{f}_\ell(\mathbf{r})$ are spatial mode functions satisfying orthonormality, and $(\hat{a}_\ell,\, \hat{a}_\ell^\dagger)$ are the time dependent annihilation and creation operators associated with each mode ℓ satisfying the canonical commutation relations

$$[\hat{a}_\ell, \hat{a}_{\ell'}^\dagger] = \delta_{\ell\ell'}, \quad [\hat{a}_\ell, \hat{a}_{\ell'}] = 0, \quad [\hat{a}_\ell^\dagger, \hat{a}_{\ell'}^\dagger] = 0$$

Fock states

In this description of the optical field, each mode ℓ is modeled as a quantum harmonic oscillator with a discrete set of energy eigenstates known as *Fock states* or number states, denoted $|n_\ell\rangle$. These states form an orthonormal basis and satisfy $\hat{n}_\ell\,|n_\ell\rangle = n_\ell\,|n_\ell\rangle$, where $\hat{n}_\ell$ is the number operator defined by

$$\hat{n}_\ell = \hat{a}_\ell^\dagger \hat{a}_\ell.$$

The action of the creation and annihilation operators on these states is given by

$$\hat{a}_\ell\,|n_\ell\rangle = \sqrt{n_\ell}\,|n_\ell - 1\rangle\,, \quad \hat{a}_\ell^\dagger\,|n_\ell\rangle = \sqrt{n_\ell + 1}\,|n_\ell + 1\rangle\,.$$

They allow transitions between Fock states by lowering or raising the photon number in mode ℓ by one unit. The vacuum state $|0_\ell\rangle$ is annihilated by $\hat{a}_\ell$, satisfying $\hat{a}_\ell\,|0_\ell\rangle = 0$. Thus, the Hamiltonian for the electromagnetic field becomes a sum of harmonic oscillator energies:

$$\hat{H} = \sum_{\ell} \hbar\omega_\ell \left(\hat{n}_\ell + \frac{1}{2}\right) \tag{II.2}$$

Quasi monochromatic fields

In realistic optical systems such as lasers, the electromagnetic field is rarely perfectly monochromatic. Instead, it exhibits a finite spectral linewidth due to stimulated emission, phase noise, or intentional modulation. These effects cause the amplitude and phase of the optical field to evolve slowly compared to the optical frequency ω_ℓ.

As a result, the complex amplitude associated with each mode, typically captured by the Heisenberg-picture annihilation operator $\hat{a}_\ell(t)$, acquires an explicit time dependence beyond the standard fast-oscillating term $e^{-i\omega_\ell t}$. This slow temporal variation reflects the underlying physics: for instance, amplitude or phase modulation, feedback-induced dynamics, or noise processes can all modulate the quantum state in time. Consequently, in the quasi-monochromatic regime, one often separates the field into a rapidly oscillating carrier and a slowly varying envelope encoded in $\hat{a}_\ell(t)$, allowing a spectrally resolved yet temporally adaptive description of the field.

Linearization of the optical field: mean field and fluctuations

We often consider a single spatial mode of the electromagnetic field with optical frequency ω_0, and assume the presence of a strong coherent field. In this regime, the annihilation operator is decomposed as $\hat{a}(t) = \bar{\alpha}(t) + \delta\hat{a}(t)$, where $\bar{\alpha}(t) = \langle \hat{a}(t) \rangle$ is a classical complex amplitude and $\delta\hat{a}(t)$ represents quantum fluctuations such that $\langle \delta\hat{a}(t) \rangle = 0$. Linearizing the electric field operator then yields:

$$\begin{aligned} \hat{\mathbf{E}}(\mathbf{r},t) = i\,\mathcal{E}\left[\bar{\alpha}(t)\,\mathbf{f}(\mathbf{r})\,e^{-i\omega_0 t} - \bar{\alpha}^*(t)\,\mathbf{f}^*(\mathbf{r})\,e^{i\omega_0 t}\right] \\ + i\,\mathcal{E}\left[\delta\hat{a}(t)\,\mathbf{f}(\mathbf{r})\,e^{-i\omega_0 t} - \delta\hat{a}^\dagger(t)\,\mathbf{f}^*(\mathbf{r})\,e^{i\omega_0 t}\right] \end{aligned} \tag{II.3}$$

The first line represents the field classical component, involving the coherent amplitude $\bar{\alpha}(t)$, while the second shows the quantum fluctuation term $\delta\hat{a}(t)$. This linearization simplifies the analysis of the field, allowing us to treat the coherent part as a classical field and the fluctuations as a quantum harmonic oscillator. The field Hamiltonian then reduces to a single-mode harmonic oscillator form:

$$\hat{H} = \hbar\omega_0\left(\delta\hat{a}^\dagger\delta\hat{a} + \frac{1}{2}\right), \tag{II.4}$$

where $\delta\hat{a}$ is the annihilation operator for the fluctuations. The coherent part contributes a constant energy offset, while the fluctuations behave as a quantum harmonic oscillator with frequency ω_0. This Hamiltonian now features an explicit time dependence through the coherent amplitude $\bar{\alpha}(t)$, which can vary slowly compared to the optical frequency. Importantly, the fluctuation operators retain the canonical bosonic commutation relations:

$$[\delta\hat{a}(t), \delta\hat{a}^\dagger(t)] = 1, \qquad [\delta\hat{a}(t), \delta\hat{a}(t)] = 0, \qquad [\delta\hat{a}^\dagger(t), \delta\hat{a}^\dagger(t)] = 0.$$

These ensure that the quantized nature of the field is preserved under linearization, with $\delta\hat{a}(t)$ and $\delta\hat{a}^\dagger(t)$ obeying the same algebra as the original field operators. The number operator can then be written as the sum of a constant (mean) part and a fluctuation part:

$$\hat{n}(t) = \hat{a}^\dagger(t)\hat{a}(t) = |\bar{\alpha}(t)|^2 + \bar{\alpha}^*(t)\delta\hat{a}(t) + \bar{\alpha}(t)\delta\hat{a}^\dagger(t) + \delta\hat{a}^\dagger(t)\delta\hat{a}(t) \tag{II.5}$$

where the constant (mean) part is simply

$$\bar{n}(t) = |\bar{\alpha}(t)|^2 \tag{II.6}$$

and the remaining terms describe the quantum fluctuations around this mean.

Remarks:

- The linearization procedure is valid when the coherent amplitude $\bar{\alpha}(t)$ is much larger than the quantum fluctuations, i.e., $|\bar{\alpha}(t)| \gg \langle \delta\hat{a}^\dagger \delta\hat{a} \rangle^{1/2}$.
- This approach is widely used in quantum optics and optomechanics to simplify the analysis of systems driven by strong gaussian fields, such as cohernet or squeezed lasers.
- The separation into mean field and fluctuations allows us to treat the quantum noise properties independently from the classical dynamics.
- The quantum fluctuation operators $\delta\hat{a}(t)$ describe vacuum or squeezed noise, and their statistics determine the ultimate sensitivity limits in measurement schemes.
- Linearization is the starting point for deriving quantum Langevin equations and for analyzing noise spectra in optomechanical systems.

Quadrature Operators

To describe the phase space properties of a field mode, we define the Hermitian quadrature operators $\hat{a}_1$ and $\hat{a}_2$ as

$$\begin{aligned} \hat{a}_1 &= \hat{a} + \hat{a}^\dagger \\ \hat{a}_2 &= \hat{a} - \hat{a}^\dagger \end{aligned} \tag{II.7}$$

More generally we can define arbitrary quadrature operators as

$$\begin{aligned} \hat{a}_\theta &= e^{i\theta}\hat{a} + e^{-i\theta}\hat{a}^\dagger \\ &= \cos\theta \hat{a}_1 + \sin\theta \hat{a}_2 \end{aligned} \tag{II.8}$$

where we notice that $\hat{a}_1 = \hat{a}_{\theta=0}$ and $\hat{a}_1 = \hat{a}_{\theta=\pi/2}$. These are Hermitian operators corresponding to measurable observables and satisfy the commutation relation

$$[a_\theta, a_{\theta+\pi/2}] = 2i \tag{II.9}$$

Uncertainty Principle and Quantum Noise

For two generic Hermitian operators $\hat{A}$ and $\hat{B}$, the Heisenberg uncertainty principle reads as

$$\Delta\hat{A}\Delta\hat{B} \geq \frac{1}{2}|[\hat{A}, \hat{B}]| \tag{II.10}$$

where we define $\Delta\hat{A} = \sqrt{|\langle \hat{A}^2 \rangle - \langle \hat{A} \rangle^2|}$. This defines the minimum amount of quantum noise (vacuum fluctuations) in the electromagnetic field. Applying this equation to the quadratures defined above we get

$$\begin{aligned} \Delta\hat{a}_1\Delta\hat{a}_2 &\geq 1 \\ \Delta\hat{a}_\theta\Delta\hat{a}_{\theta+\pi/2} &\geq 1 \end{aligned} \tag{II.11}$$

We now turn to standard optical quantum states, in particular gaussian states i.e. full positive in Wigner functin representations such as coherent and squeezed states, that we will denote in braket notation as $\langle \alpha \rangle$ and $|\alpha, \xi\rangle$.

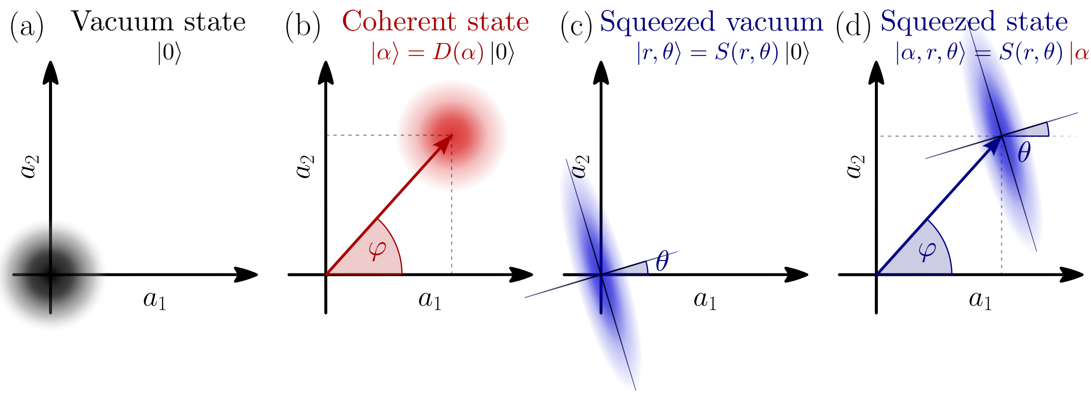
(a) Vacuum state
$|0\rangle$
(b) Coherent state
$|\alpha\rangle = D(\alpha)\,|0\rangle$
(c) Squeezed vacuum
$|r,\theta\rangle = S(r,\theta)\,|0\rangle$
(d) Squeezed state
$|\alpha,r,\theta\rangle = S(r,\theta)\,|\alpha\rangle$
a_2
a_1
φ
θ

Fig. II.1 *Phase-space representations of quantum states and transformations. (a) Wigner function of the vacuum state: a circular Gaussian centered at the origin, representing equal quantum fluctuations in both quadratures* a_1 *and* a_2*. (b) Wigner function of a coherent state: a displaced circular Gaussian, showing a shift in phase space along an angle* φ *with unchanged, isotropic noise. (c) Wigner function of a squeezed vacuum state: an elliptical Gaussian centered at the origin, with reduced noise along a rotated quadrature* X_θ *and increased noise in the orthogonal direction. (d) Wigner function of a displaced squeezed state: an ellipse shifted away from the origin, combining anisotropic fluctuations and a nonzero mean amplitude. The displacement angle* φ *and squeezing angle* θ *are independent.*

Coherent States

The coherent state $\langle\alpha\rangle$ is an eigenstate of the annihilation operator:

$$\hat{a}|\alpha\rangle = \alpha|\alpha\rangle \tag{II.12}$$

And can be expressed in the Fock basis as:

$$|\alpha\rangle = e^{-|\alpha|^2/2}\sum_{n=0}^{\infty}\frac{\alpha^n}{\sqrt{n!}}|n\rangle \tag{II.13}$$

and are generated by the action of the displacement operator $\hat{D}(\alpha)$ on the vacuum state $|0\rangle$:

$$|\alpha\rangle = \hat{D}|0\rangle, \quad \hat{D}(\alpha) = \exp\Big(\alpha\hat{a}^\dagger - \alpha^*\hat{a}\Big) \tag{II.14}$$

For a coherent state $|\alpha\rangle$, the expectation values and variances of the quadrature operators are:

$$\begin{aligned}\langle\hat{a}_\theta\rangle &= 2\,\mathrm{Re}(\alpha e^{i\theta})\\ \Delta\hat{a}_\theta^2 &= 1\end{aligned} \tag{II.15}$$

That is, the mean value of any quadrature is set by the coherent amplitude, while the variance is unity (in these units) for all quadratures. The mean photon number in a coherent state is given by:

$$\langle\hat{N}\rangle = \langle\alpha|\hat{a}^\dagger\hat{a}|\alpha\rangle = |\alpha|^2 \tag{II.16}$$

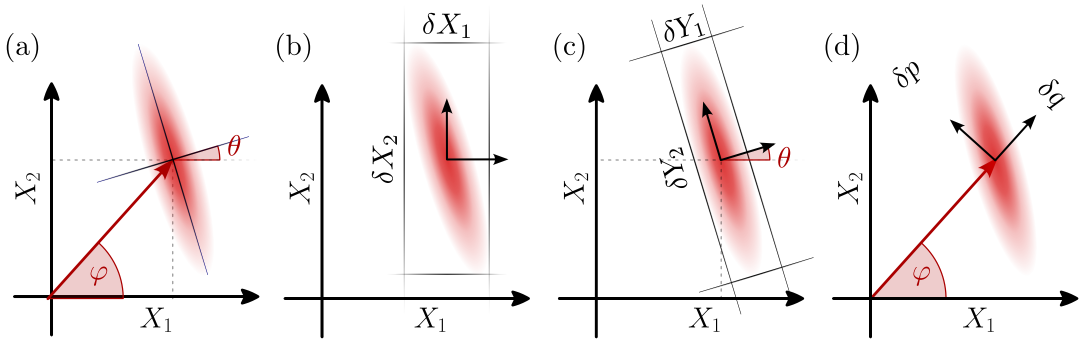

Fig. II.2 *Phase-space representations of quantum states and transformations. (a) Wigner function of the vacuum state: a circular Gaussian centered at the origin, representing equal quantum fluctuations in both quadratures X_1 and X_2. (b) Wigner function of a coherent state: a displaced circular Gaussian, showing a shift in phase space along an angle φ with unchanged, isotropic noise. (c) Wigner function of a squeezed vacuum state: an elliptical Gaussian centered at the origin, with reduced noise along a rotated quadrature X_θ and increased noise in the orthogonal direction. (d) Wigner function of a displaced squeezed state: an ellipse shifted away from the origin, combining anisotropic fluctuations and a nonzero mean amplitude. The displacement angle φ and squeezing angle θ are independent.*

Coherent states are often referred to as "classical" states of light because they exhibit Poissonian photon statistics and minimal uncertainty in phase space, making them the closest quantum analog to classical electromagnetic waves. They are widely used in quantum optics and form the basis for many experimental techniques.

Squeezed States

Squeezed states $|\alpha, \xi\rangle$ are quantum states of light in which the noise (variance) of one quadrature is reduced below the vacuum level, at the expense of increased noise in the conjugate quadrature. The single-mode squeezed vacuum state is defined as

$$|0, \xi\rangle = \hat{S}(\xi)|0\rangle \tag{II.17}$$

$$\hat{S}(\xi) = \exp\left[\frac{1}{2}(\xi^* \hat{a}^2 - \xi \hat{a}^{\dagger 2})\right], \quad \xi = re^{i\phi} \tag{II.18}$$

where r is the squeezing parameter (strength) and ϕ is the squeezing angle. For $\phi = 0$ (amplitude quadrature squeezing), the quadrature variances become

$$\Delta X_1 = \frac{e^{-r}}{\sqrt{2}}, \qquad \Delta X_2 = \frac{e^{r}}{\sqrt{2}} \tag{II.19}$$

where $X_1 = (\hat{a} + \hat{a}^\dagger)$ and $X_2 = -i(\hat{a} - \hat{a}^\dagger)$ are the amplitude and phase quadratures, respectively.

The most general Gaussian state is the displaced squeezed state, obtained by applying both the squeezing operator $\hat{S}(\xi)$ and the displacement operator $\hat{D}(\alpha)$ to the vacuum:

$$|\alpha, \xi\rangle = \hat{D}(\alpha)\hat{S}(\xi)|0\rangle \tag{II.20}$$

where $\hat{D}(\alpha) = \exp\Big(\alpha\hat{a}^\dagger - \alpha^*\hat{a}\Big)$ displaces the state in phase space by the complex amplitude α.

Note: The displacement and squeezing operators do not commute, i.e., $\hat{D}(\alpha)\hat{S}(\xi) \neq \hat{S}(\xi)\hat{D}(\alpha)$. However, both orderings correspond to experimentally valid procedures: one can either squeeze the vacuum and then displace (e.g., by mixing with a coherent state), or first generate a bright coherent state (e.g., by seeding an optical parametric amplifier) and then squeeze it. The resulting state is always a displaced squeezed state, but the relative phase between displacement and squeezing may differ. where their respective product satisfies the Heisenberg uncertainty relation. Moreover the mean photon number in the squeezed state is:

$$\langle\hat{N}\rangle = \langle\alpha, \xi|\hat{a}^\dagger\hat{a}|\alpha, \xi\rangle = |\alpha|^2 + \sinh^2 \tag{II.21}$$

This shows that the squeezing operation increases the mean photon number of the coherent state by adding photons. Physically, this reflects the fact that generating squeezed light requires injecting energy into the system, so the squeezed vacuum contains correlated field excitations (photons) in even numbers. This is further illustrated by the two-mode squeezing operator, which describes the simultaneous creation or annihilation of photon pairs in two modes (such as upper and lower sidebands or two distinct modes):

$$\hat{S}_2(\xi) = \exp\left[\xi^*\hat{a}_+\hat{a}_- - \xi\hat{a}_+^\dagger\hat{a}_-^\dagger\right], \quad \xi = re^{i\phi} \tag{II.22}$$

The expectation values of the annihilation operators $\hat{a}_+$ and $\hat{a}_-$ in a two-mode squeezed vacuum state $|\xi\rangle = \hat{S}_2(\xi)|0\rangle$ are both zero:

$$\langle\xi|\hat{a}_+|\xi\rangle = 0, \qquad \langle\xi|\hat{a}_-|\xi\rangle = 0 \tag{II.23}$$

This reflects that the two-mode squeezed vacuum has zero mean field in both modes. However, the expectation value of the product $\hat{a}_+\hat{a}_-$ is nonzero:

$$\langle\xi|\hat{a}_+\hat{a}_-|\xi\rangle = -e^{i\phi}\sinh r\cosh r \tag{II.24}$$

where $\xi = re^{i\phi}$ is the squeezing parameter. This nonzero correlation is a hallmark of two-mode squeezing and underlies quantum entanglement between the modes. This form describes two-mode squeezing, where photon pairs are created or annihilated simultaneously in the $+$ and $-$ modes. For $\phi = 0$, the squeezing is along the amplitude quadrature; for $\phi = \pi/2$, along the phase quadrature. This operator is central to the description of squeezed vacuum states generated by parametric down-conversion and is widely used in quantum optics and optomechanics.

In quantum optics, a two-mode squeezed vacuum state arises from the parametric down-conversion of a pump field at frequency 2ω, producing pairs of photons at symmetric sideband frequencies $\omega \pm \Omega$. The resulting state is a pure entangled superposition of twin Fock states, of the form

$$|\psi\rangle = \sum_{n=0}^{\infty} c_n\,|n\rangle_+ \otimes |n\rangle_-, \quad \text{with} \quad c_n \propto \tanh^n r,$$

where r is the squeezing parameter. Importantly, when one sideband is traced out, the reduced state of the remaining mode becomes a thermal state with a Bose-Einstein photon number distribution

$$P_n = \frac{\bar{n}^n}{(\bar{n}+1)^{n+1}}, \quad \text{with} \quad \bar{n} = \sinh^2 r.$$

This thermal character is not due to any external bath but results from quantum entanglement and the loss of information associated with ignoring one mode of the pair. The corresponding Wigner function is isotropic and broader than that of vacuum, with quadrature variances

$$\langle \hat{X}^2 \rangle = \langle \hat{Y}^2 \rangle = \bar{n} + \frac{1}{2},$$

reflecting excess fluctuations in all directions of phase space. In contrast, a single-mode squeezed vacuum involves an even-parity superposition,

$$|\xi\rangle = \sum_{n=0}^{\infty} d_{2n} \, |2n\rangle,$$

resulting from the same parametric process but in a degenerate configuration where photons are created in indistinguishable pairs. While single-mode squeezing yields quadrature-dependent noise (an elliptical Wigner function), its photon statistics also reveal the underlying pairwise structure of the interaction. Crucially, both processes involve the coherent transformation of vacuum fluctuations rather than thermal excitations. At optical frequencies ($\omega \sim 300\,\mathrm{THz}$) and room temperature ($T = 300\,\mathrm{K}$), the thermal occupation

$$\bar{n}_{\text{th}} = \frac{1}{e^{\hbar\omega/k_B T} - 1} \sim 10^{-20}$$

is entirely negligible. This stark contrast between thermal and quantum (entanglement-induced) noise is essential to interpreting squeezed state measurements and correctly identifying the quantum origin of excess fluctuations observed in individual modes.

This concludes our introduction to the quantum description of light, setting the stage for modelling interactions between quantum optical fields and mechanical resonators.

II.1.2 Optical Field Modulations

Linearization of the Electric Field and Modulation Sidebands

We consider a single optical mode with a strong coherent drive. The annihilation operator is linearized as:

$$\hat{a}(t) \to \bar{\alpha}(t) + \delta\hat{a}(t) \tag{II.25}$$

where $\bar{\alpha}(t) \in \mathbb{C}$ is the classical coherent amplitude and $\delta\hat{a}(t)$ captures quantum fluctuations. When considering optical features of the quantized electric field, it is common to drop the spatial mode functions $\mathbf{f}(\mathbf{r})$ and $\mathbf{f}^*(\mathbf{r})$ for simplicity, focusing on the time-dependent coherent amplitude $\bar{\alpha}(t)$ and its complex conjugate $\bar{\alpha}^*(t)$. This makes the notation slightly lighter and the classical part of the electric field operator can then be expressed as:

$$\mathbf{E}_{\text{cl}}(t) = i\sqrt{\frac{\hbar\omega_0}{2\varepsilon_0}} \left[\bar{\alpha}(t)\, e^{-i\omega_0 t} - \bar{\alpha}^*(t)\, e^{i\omega_0 t} \right] \tag{II.26}$$

where we dropped the spatial degree of freedom in for clarity.

We now consider two types of sinusoidal modulation at frequency Ω:

Amplitude Modulation (AM)

Let the coherent amplitude be modulated in amplitude:

$$\bar{\alpha}(t) = \bar{\alpha}_0 \left(1 + \epsilon_a \cos(\Omega t)\right) \tag{II.27}$$

with $\epsilon_a \ll 1$, the field amplitude modulation depth. Substituting into the field expression and dropping the spatial mode functions for clarity:

$$\begin{aligned} E_{\mathrm{cl}}^{(\mathrm{AM})}(t) = i\sqrt{\frac{\hbar\omega_0}{2\varepsilon_0}}\,\bar{\alpha}_0 \Big[& \underbrace{e^{-i\omega_0 t} - e^{i\omega_0 t}}_{\text{carrier}} \\ & + \underbrace{\frac{\epsilon_a}{2}\left(e^{-i(\omega_0-\Omega)t} - e^{i(\omega_0-\Omega)t}\right)}_{\text{lower sideband } (\omega_0-\Omega)} \\ & + \underbrace{\frac{\epsilon_a}{2}\left(e^{-i(\omega_0+\Omega)t} - e^{i(\omega_0+\Omega)t}\right)}_{\text{upper sideband } (\omega_0+\Omega)} \Big] \end{aligned} \tag{II.28}$$

Phase Modulation (PM)

Now consider phase modulation of the coherent amplitude:

$$\bar{\alpha}(t) = \bar{\alpha}_0 e^{i\epsilon_\phi \cos(\Omega t)} \approx \bar{\alpha}_0 \left(1 + i\epsilon_\phi \cos(\Omega t)\right) = \bar{\alpha}_0 \left(1 + \frac{i\epsilon_\phi}{2} e^{i\Omega t} + \frac{i\epsilon_\phi}{2} e^{-i\Omega t}\right) \tag{II.29}$$

with $\epsilon_\phi \ll 1$, the field phase modulation depth. Substituting into the field expression and dropping the spatial mode functions:

$$\begin{aligned} E_{\mathrm{cl}}^{(\mathrm{PM})}(t) = i\sqrt{\frac{\hbar\omega_0}{2\varepsilon_0}}\,\bar{\alpha}_0 \Big[& \underbrace{e^{-i\omega_0 t} - e^{i\omega_0 t}}_{\text{carrier}} \\ & + \underbrace{\frac{i\epsilon_\phi}{2}\left(e^{-i(\omega_0-\Omega)t} + e^{i(\omega_0-\Omega)t}\right)}_{\text{lower sideband } (\omega_0-\Omega)} \\ & + \underbrace{\frac{i\epsilon_\phi}{2}\left(e^{-i(\omega_0+\Omega)t} + e^{i(\omega_0+\Omega)t}\right)}_{\text{upper sideband } (\omega_0+\Omega)} \Big] \end{aligned} \tag{II.30}$$

Interpretation

In both cases, the field contains a carrier at frequency ω and two sidebands at $\omega \pm \Omega$. Amplitude modulation results in sidebands that are in phase with the carrier, while phase modulation produces sidebands with a $\pm\pi/2$ phase shift relative to the carrier.

II.1.3 Quantum Noise and Uncertainty

II.1.4 Sideband Representation

We begin by recalling the quantized electric field operator for a single spatial mode with carrier frequency ω_0 and mode function $\mathbf{f}(\mathbf{r})$ (as in Eq. II.1):

$$\hat{\mathbf{E}}(\mathbf{r},t) = i\mathcal{E}\left[\hat{a}(t)\,\mathbf{f}(\mathbf{r})\,e^{-i\omega_0 t} - \hat{a}^\dagger(t)\,\mathbf{f}^*(\mathbf{r})\,e^{i\omega_0 t}\right] \tag{II.31}$$

where $\hat{a}(t)$ is the slowly varying annihilation operator in the rotating frame. To analyze the field in the sideband representation, we express the annihilation operator in terms of its Fourier components over positive frequencies:

$$\hat{a}(t) = \int_0^\infty \frac{d\omega}{2\pi}\,\hat{a}(\omega)e^{-i\omega t} \tag{II.32}$$

We introduce a central carrier frequency ω_0 and define sideband frequencies via $\Omega = \omega_0 - \omega$. Furthermore, we assume that the field is band-limited to a finite bandwidth B around the carrier frequency, which reduces the shifted range of integration to :

$$\omega \in [0,\infty[\quad \Rightarrow \quad \Omega \in [-\omega_0,\infty[\quad \Rightarrow \quad \Omega \in [-B,B[$$

so that the expression reduces to

$$\hat{a}(t) = e^{-i\omega_0 t}\int_{-B}^{B} \frac{d\Omega}{2\pi}\,\hat{a}_+(\Omega)e^{-i(\Omega)t} \tag{II.33}$$

where we defined the sideband annihilation operators:

$$\hat{a}_+(\Omega) := \hat{a}(\omega_0+\Omega), \quad \hat{a}_-(\Omega) := \hat{a}(\omega_0-\Omega) \tag{II.34}$$

The above field expression is then succintly written as:

$$\hat{a}(t) = e^{-i\omega_0 t}\int_0^B \frac{d\Omega}{2\pi}\left[\hat{a}_+(\Omega)e^{-i\Omega t} + \hat{a}_-(\Omega)e^{i\Omega t}\right] \tag{II.35}$$

II.2 Optical Cavities: Basics

II.2.1 Cavity types and Resonance Conditions

II.2.2 Spatial and Longitudinal Modes

II.2.3 Quantum Langevin Equations

We consider a bosonic mode described by the annihilation operator $\hat{a}(t)$, interacting with several independent Markovian reservoirs. The system is governed by a Hamiltonian $\hat{H}_{\text{sys}}$, and each reservoir introduces dissipation characterized by a decay rate κ_i. In the Heisenberg picture, the dynamics of $\hat{a}(t)$ is given by the quantum Langevin equation:

$$\frac{d}{dt}\hat{a}(t) = -i[\hat{a},\hat{H}_{\text{sys}}] - \frac{\kappa}{2}\hat{a}(t) + \sum_i \sqrt{\kappa_i}\,\hat{a}_{\text{in},i}(t), \tag{II.36}$$

where:

- $\kappa = \sum_i \kappa_i$ is the total decay rate,
- $\hat{a}_{\mathrm{in},i}(t)$ are the input noise operators associated with each reservoir.

The input fields $\hat{a}_{\mathrm{in},i}(t)$ model quantum fluctuations entering the system from each bath. For uncorrelated reservoirs in the vacuum state, these noise operators satisfy the following correlation and commutation relations:

$$\left[\hat{a}_{\mathrm{in},i}(t), \hat{a}^{\dagger}_{\mathrm{in},j}(t')\right] = \delta_{ij}\,\delta(t-t'), \tag{II.37}$$

$$\langle \hat{a}_{\mathrm{in},i}(t)\hat{a}^{\dagger}_{\mathrm{in},j}(t')\rangle = \delta_{ij}\,\delta(t-t'), \tag{II.38}$$

$$\langle \hat{a}^{\dagger}_{\mathrm{in},i}(t)\hat{a}_{\mathrm{in},j}(t')\rangle = 0. \tag{II.39}$$

Equation (II.36) encapsulates the interplay between coherent evolution driven by the system Hamiltonian, dissipation into multiple channels, and quantum noise introduced by each reservoir. This structure is particularly relevant in cavity and circuit quantum electrodynamics, where a single bosonic mode (e.g., an optical or microwave cavity) is simultaneously coupled to several loss ports (e.g., transmission lines, internal losses, or detection chains).

II.3 Optical Cavities: Three Mirror Cavities

II.3.1

II.4 Cavity Optomechanics

II.4.1 Radiation Pressure Coupling

II.4.2 Quantum Langevin Equations

II.4.3 Mechanical Resonators

Mechanical Resonators

II.4.4 Noise spectra

II.4.5 Three Mirror Cavities as Novel Optomechanical Systems

II.5 Squeezed Light Theory

II.5.1 Single-mode Squeezing

II.5.2 Noise Spectra

II.5.3 Frequency-dependent Squeezing and its use

II.6 Numerical Methods and Simulations

Chapter III

Experimental Methods

This chapter will cover the experimental methods used in the development of optomechanical systems, focusing on the generation of squeezed light and the techniques for optical locking and quadrature measurement. The methods are designed to enhance the sensitivity of measurements in quantum optics and optomechanics.

Contents

III.1 Optical Locking Techniques with PyRPL 18
  III.1.1 Proportion-Integral (PI) Controllers 18
  III.1.2 Temperature Locks 19
  III.1.3 Optical paths Locks 20
  III.1.4 Side of Fringe Locks 20
  III.1.5 Pound-Drever-Hall Locks 20
  III.1.6 Offset frequency Locks 22
  III.1.7 Coherent Sideband Locks 22
  III.1.8 PyRPL Control Implementation 22
III.2 Optical Cavities and Squeezed Light Generation 22
  III.2.1 Cavity Types and Alignement Procedures 22
  III.2.2 Bowtie-type Optical Parametric Oscillator (OPO) 22
  III.2.3 Phase Matching and Nonlinear Crystals 22
  III.2.4 Filter Cavities for Squeezing Rotation 22
III.3 Quadrature Measurement Techniques 22
  III.3.1 Direct Detection with Photodiodes 22
  III.3.2 Balanced Homodyne Detection 22
  III.3.3 Local Oscillator Design and Control 22

III.1 Optical Locking Techniques with PyRPL

A central aspect of the experimental setups is the ability to stabilize various optical features. In this work, it is the case for the relative phase between two optical paths, keeping optical cavities on resonance, or fixing the detuning between a master and a slave laser.

This section will cover the locking techniques used in this work, from basic Michelson-type locking to more advanced Pound-Drever-Hall techniques and phase-locked loops. The implementation of these techniques using the in-house library PyRPL is presented.

III.1.1 Proportion-Integral (PI) Controllers

Proportional-Integral (PI) controllers are widely used in quantum optics experiments to stabilize critical parameters such as cavity length, laser frequency, and optical phase. To this end, one needs to extract an error signal $\epsilon(t)$ that quantifies the deviation from a desired setpoint, such as a target temperature, phase difference or cavity resonance. It is typically expressed as the difference between a measured signal and its reference value:

$$\epsilon(t) = s_{\text{meas}}(t) - s_{\text{ref}},$$

where $s_{\text{meas}}(t)$ denotes the physical quantity monitored in the experiment (e.g., reflected intensity or interferometric signal), and s_{ref} is the target value corresponding to the lock point.

For effective feedback stabilization, the error signal must satisfy several essential criteria:

- **High SNR:** Near the setpoint, $\epsilon(t)$ should exhibit a high SNR to ensure robust locking and minimize the influence of technical and electronic noise.
- **Linearity and antisymmetry:** The error signal should be linear and antisymmetric in a neighborhood of the operating point. Small deviations from the setpoint should produce a proportional response in $\epsilon(t)$, with opposite signs for deviations of opposite direction.
- **Monotonicity and uniqueness:** The slope $\partial\epsilon/\partial x$, where x denotes the control parameter (e.g., cavity length or laser frequency), should be monotonic and unambiguous near the lock point to avoid multiple equilibrium points and ensure stable locking behavior.
- **Steep slope near the setpoint:** A steeper slope improves sensitivity to small deviations and enhances lock accuracy, although it must be balanced against potential noise amplification.
- **Bandwidth compatibility:** The spectral content of $\epsilon(t)$ must be compatible with the bandwidth of the actuator and the dynamics of the system. For example, in the case of a piezoelectric transducer, which acts as a low-pass mechanical element, the error signal high-frequency components won't be compensated by the actuator.

The PI controller computes the feedback signal $u(t)$ from the error signal $\epsilon(t)$ according to:

$$u(t) = K_P \, \epsilon(t) + K_I \int_0^t \epsilon(\tau) d\tau \tag{III.1}$$

where K_P and K_I are the proportional and integral gains, respectively. The proportional term $K_P \, e(t)$ responds to the current error and primarily acts on mid-frequency deviations, enabling rapid corrections. The integral term $K_I \int \epsilon(\tau) d\tau$ accumulates past errors and is most effective at low frequencies, helping to eliminate long-term drifts and steady-state offsets.

In classical control theory, PID (Proportional-Integral-Derivative) controllers are designed to stabilize dynamic systems by combining three terms: a proportional term for immediate response, an integral term to eliminate steady-state error, and a derivative term that anticipates future error based on the rate of change. However, in practical experimental setups—particularly in quantum optics—PI control (Proportional-Integral) is typically sufficient and even preferable to full PID control. The derivative term, which acts predominantly at high frequencies, is generally unnecessary and can be counterproductive. This is because the feedback actuator is often a piezoelectric transducer, which exhibits non-zero capacitance. Combined with the finite output impedance of the control electronics, this forms a natural low-pass filter that significantly attenuates high-frequency components of the feedback signal. As a result, any derivative term—which primarily targets high-frequency correction—would be both ineffective due to this filtering and potentially harmful by injecting high-frequency noise into the loop.

Therefore, PI control offers a balanced and robust approach: the integral term suppresses low-frequency drifts (typically below a few Hz to tens of Hz), the proportional term corrects intermediate-frequency deviations (up to a few kHz), and high-frequency components (above the mechanical resonance or actuation bandwidth) are naturally filtered out and deliberately left uncorrected. This allows for stable feedback while preserving high-frequency signals—such as thermal noise or mechanical sidebands—which carry essential physical information for analysis and measurement.

III.1.2 Temperature Locks

A first example of a PI lock used in this work is the temperature lock, which is used to stabilize the temperature of non linear crystals embedded inside optical cavities. The error signal is derived from a temperature sensor, such as a thermistor, which measures the temperature of the crystal. The error signal is then fed into a PI controller, which adjusts the heating element, a peltier module in our case, to maintain the desired temperature setpoint.

The temperature lock is crucial for maintaining the phase matching conditions in nonlinear optical processes (developped in the next section), such as second-harmonic generation or optical parametric oscillation, where the efficiency of frequency conversion depends sensitively on the crystal temperature. By stabilizing the temperature, we ensure that the nonlinear interactions remain optimal, leading to consistent and reproducible results in experiments involving squeezed light generation or other nonlinear optical phenomena.

III.1.3 Optical paths Locks

Controlling the relative path length between two arms of an interferometer is a fundamental technique in quantum optics. The basic idea is to use the interference of light from two paths to lock the phase difference between them. Although not being the same experiental setups, Michelson interferometers, Mach-Zhender interferometers, and Local Oscillator stabilization error signals fall in the same category as they are derived from the same principle. Namely, the error signal is proportional to the sine of the phase difference between the two arms:

$$\epsilon(\Delta\phi) \propto \sin(\Delta\phi) \tag{III.1}$$

where $\Delta\phi = \phi_a - \phi_b$ is the phase difference between the two optical paths. Analogically, we would need to add an adjustable voltage offset, as to be able to tune the error signal to zero at the desired phase difference, before seeding this error signal to the PI block. Digitally, this is performed by adding a constant offset to the error signal, which can be adjusted to set the desired phase difference.

In practice, this is implemented by mounting a mirror on which one of the arms is reflected, and then using a piezoelectric transducer to control the position of the mirror, hence modulating the relative phase between the two optical paths. The piezo is then feedback controlled through a PI loop, which adjusts the voltage applied to the piezo to set the error signal to 0. FIGURE

III.1.4 Side of Fringe Locks

III.1.5 Pound-Drever-Hall Locks

Another key technique extensively used in this work is the *Pound-Drever-Hall* (PDH) method, a high-sensitivity scheme for stabilizing either the cavity length to a fluctuating laser frequency, or vice versa. The method relies on imposing phase modulation sidebands on the laser field, typically using an electro-optic modulator (EOM), and using these sidebands as phase-stable references. Because they lie far outside the cavity linewidth ($\Omega_{\mathrm{mod}} \gg \kappa$), the sidebands are reflected nearly unchanged: $r(\omega_\ell \pm \Omega_{\mathrm{mod}}) \approx 1$. In contrast, the carrier field near resonance acquires a frequency-dependent phase shift upon reflection, captured by the complex cavity reflection coefficient $r_c(\delta)$. The PDH error signal is obtained by detecting the reflected beam and demodulating the photocurrent at the modulation frequency, isolating the beat terms between carrier and sidebands. The resulting signal is proportional to the *imaginary part* of $r_c(\delta)$, which varies antisymmetrically with detuning and provides a zero-crossing error signal ideal for linear feedback. This imaginary component encodes the rapid phase dispersion near resonance that allows the system to discriminate the sign and magnitude of frequency deviations. In contrast, the real part of $r_c(\delta)$, being symmetric around resonance, does not yield a usable error signal.

The *demodulation phase* plays a critical role in selecting the appropriate quadrature of the signal for feedback. Since the beat signal between the carrier and sidebands has both in-phase (cosine) and quadrature (sine) components, choosing the correct demodulation phase ensures that the extracted error signal aligns with the imaginary part of the reflection coefficient. A misaligned demodulation phase can lead to mixing of the symmetric (real) part into the error signal, thereby reducing sensitivity and introducing offset or distortion near the lock point. In practice, the demodulation phase is optimized empirically—either via a variable phase shifter in the electronic demodulation path or by adjusting the physical delay in the reference oscillator—to maximize the slope of the error signal at zero-crossing, corresponding to pure detection of the dispersive component.

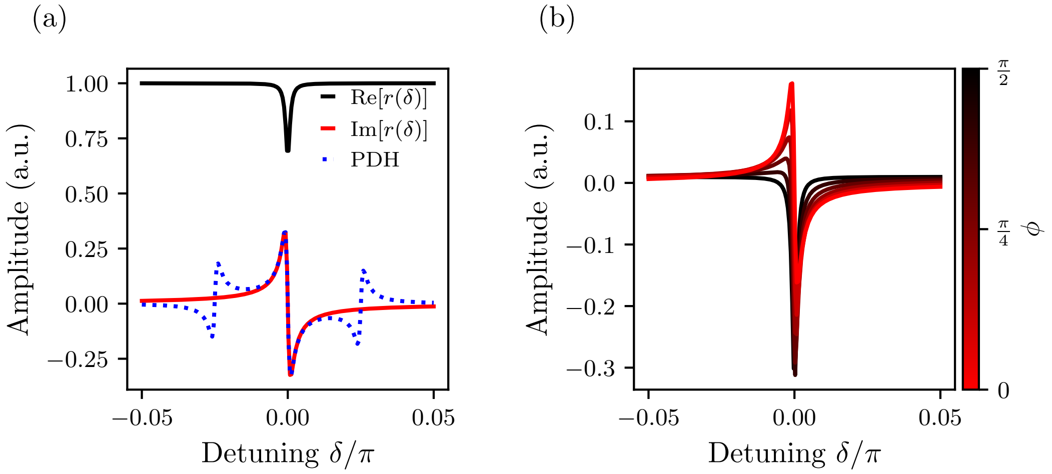

Fig. III.1 *Schematic of the Pound-Drever-Hall (PDH) locking technique. The laser passes through an electro-optic modulator (EOM) generating phase modulation sidebands. The modulated beam is incident on the optical cavity, and the reflected light is detected by a photodiode (PD). The photocurrent is demodulated at the modulation frequency to produce the PDH error signal, which is fed to a PI controller driving the cavity actuator (e.g., piezo). Key components are labeled: EOM (electro-optic modulator), PD (photodiode), LO (local oscillator for demodulation), and PI (proportional-integral controller).*

The *lock-in optical phase-sensitive error measurement* (LOPSEM) technique is a versatile method for extracting phase information from modulated optical signals. In the context of PDH locking, LOPSEM is used to demodulate the photodiode signal at the modulation frequency, isolating the dispersive error signal required for feedback. By employing a lock-in amplifier or digital demodulation, the technique enables precise selection of the signal quadrature, allowing for robust discrimination of phase shifts induced by cavity detuning. This approach enhances the sensitivity and stability of optical locks, making it an essential tool in quantum optics experiments where accurate phase control is critical.

III.1.6 Offset frequency Locks

coucou Marie

III.1.7 Coherent Sideband Locks

III.1.8 PyRPL Control Implementation

III.2 Optical Cavities and Squeezed Light Generation

Maybe I need to add a section on the theory of squeezed light generation, but for now I will just focus on the experimental methods.

III.2.1 Cavity Types and Alignement Procedures

III.2.2 Bowtie-type Optical Parametric Oscillator (OPO)

III.2.3 Phase Matching and Nonlinear Crystals

III.2.4 Filter Cavities for Squeezing Rotation

III.3 Quadrature Measurement Techniques

III.3.1 Direct Detection with Photodiodes

III.3.2 Balanced Homodyne Detection

III.3.3 Local Oscillator Design and Control

Chapter IV

Experiments: Optomechanical Three-Mirror Cavity Systems

This chapter will cover the experimental methods used in the development of optomechanical three-mirror cavity systems, focusing on the design, fabrication, and characterization of mechanical resonators within optical cavities. The methods are designed to enhance the sensitivity of measurements in quantum optics and optomechanics.

Contents

IV.1 System Description and Setup **24**
  IV.1.1 Cavity Geometry and CAD Models 24
  IV.1.2 Laser Source and Optical Layout 24
  IV.1.3 Alignment Procedures 24
IV.2 Middle Mirror as Mechanical Resonator **24**
  IV.2.1 Plane Membranes: Design and Characterization 24
  IV.2.2 Phononic Crystals: Dahlia Pattern 24
  IV.2.3 Fabrication and Performance Metrics 24
IV.3 Experimental Characterization **24**
  IV.3.1 Cavity Mode Scanning and Modematching 24
  IV.3.2 Locking Techniques and Stability 24
  IV.3.3 Ringdown Measurements and Q-factor Analysis 24
IV.4 Data Acquisition and Analysis **24**
  IV.4.1 Measurement Setup and Instrumentation 24
  IV.4.2 Spectral Acquisition and Processing 24
  IV.4.3 Feedback Control Implementation 24
IV.5 Introduction to Experimental Methods **24**
IV.6 Design of an Optomechanical Fibered Cavity **24**
  IV.6.1 Design considerations 24

IV.1 System Description and Setup

IV.1.1 Cavity Geometry and CAD Models

IV.1.2 Laser Source and Optical Layout

IV.1.3 Alignment Procedures

IV.2 Middle Mirror as Mechanical Resonator

IV.2.1 Plane Membranes: Design and Characterization

IV.2.2 Phononic Crystals: Dahlia Pattern

IV.2.3 Fabrication and Performance Metrics

IV.3 Experimental Characterization

IV.3.1 Cavity Mode Scanning and Modematching

IV.3.2 Locking Techniques and Stability

IV.3.3 Ringdown Measurements and Q-factor Analysis

IV.4 Data Acquisition and Analysis

IV.4.1 Measurement Setup and Instrumentation

IV.4.2 Spectral Acquisition and Processing

IV.4.3 Feedback Control Implementation

IV.5 Introduction to Experimental Methods

IV.6 Design of an Optomechanical Fibered Cavity

IV.6.1 Design considerations

Chapter V

Experiments: Frequency Dependent Squeezing

This chapter will cover the experimental methods used in the development of frequency-dependent squeezing in optomechanical systems, focusing on the generation of squeezed light, optical locking techniques, and quadrature measurement methods. The methods are designed to enhance the sensitivity of measurements in quantum optics and optomechanics.

Contents

V.1 OPO Resonance and Locking 26
  V.1.1 Resonance Conditions and Sweeps 26
  V.1.2 Lock Acquisition and Optimization 26
  V.1.3 Stability Characterization 26
V.2 Quadrature Spectral Analysis 26
  V.2.1 Detection of Squeezing and Anti-squeezing 26
  V.2.2 Spectral Variation with Frequency 26
  V.2.3 Optimal Quadrature Conditions 26
V.3 Filter Cavity Concept 26
  V.3.1 Virgo Filter Cavity 26
  V.3.2 Thermal effects in bichromatic locks 26
Appendix: PDH Derivation 29

V.1 OPO Resonance and Locking

V.1.1 Resonance Conditions and Sweeps

V.1.2 Lock Acquisition and Optimization

V.1.3 Stability Characterization

V.2 Quadrature Spectral Analysis

V.2.1 Detection of Squeezing and Anti-squeezing

V.2.2 Spectral Variation with Frequency

V.2.3 Optimal Quadrature Conditions

V.3 Filter Cavity Concept

V.3.1 Virgo Filter Cavity

V.3.2 Thermal effects in bichromatic locks

Summary, conclusion and perspectives

This chapter will cover the summary of the work done, the conclusions drawn from the experiments, and the perspectives for future research in optomechanical systems. It will highlight the key findings, their implications for quantum optics, and potential directions for further exploration.

Appendix: Derivation of the Pound-Drever-Hall Error Signal Using the Quantum-Normalized Electric Field

In this appendix, we derive the Pound-Drever-Hall (PDH) error signal starting from the real, quantum-normalized phase-modulated electric field expression. We aim to show how the demodulated signal is a linear combination of the real and imaginary parts of the cavity reflection coefficient, with the demodulation phase selecting the appropriate quadrature for locking.

1. Input Phase-Modulated Field

The electric field at the input of the cavity is assumed to be a coherent state that has been phase-modulated at frequency Ω, such that the classical (real) electric field takes the form:

$$E_{\mathrm{cl}}^{(\mathrm{PM})}(t) = i\sqrt{\frac{\hbar\omega_0}{2\varepsilon_0}}\,\alpha_0\left[e^{-i\omega_0 t} - e^{i\omega_0 t} + \frac{i\epsilon_\phi}{2}\left(e^{-i(\omega_0-\Omega)t} + e^{i(\omega_0-\Omega)t}\right) + \frac{i\epsilon_\phi}{2}\left(e^{-i(\omega_0+\Omega)t} + e^{i(\omega_0+\Omega)t}\right)\right] \tag{1}$$

where α_0 is the coherent amplitude of the carrier, $\epsilon_\phi \ll 1$ is a small modulation index (related to the phase modulation depth), and ω_0 is the optical carrier frequency. This field includes both the positive and negative frequency components, as expected for a physical (Hermitian) electric field operator.

2. Reflection from the Cavity

Each frequency component of the field is reflected with a complex frequency-dependent amplitude reflection coefficient $r(\omega)$, such that the reflected field is:

$$\begin{aligned} E_{\mathrm{refl}}(t) = i\sqrt{\frac{\hbar\omega_0}{2\varepsilon_0}}\,\alpha_0\Big[&r(\omega_0)e^{-i\omega_0 t} - r^*(\omega_0)e^{i\omega_0 t} \\ &+ \frac{i\epsilon_\phi}{2}\left(r(\omega_0-\Omega)e^{-i(\omega_0-\Omega)t} + r^*(\omega_0-\Omega)e^{i(\omega_0-\Omega)t}\right) \\ &+ \frac{i\epsilon_\phi}{2}\left(r(\omega_0+\Omega)e^{-i(\omega_0+\Omega)t} + r^*(\omega_0+\Omega)e^{i(\omega_0+\Omega)t}\right)\Big] \end{aligned} \tag{2}$$

3. Photodetected Intensity

The photodetector measures the intensity:

$$I(t) \propto |E_{\text{refl}}(t)|^2$$

We isolate the terms oscillating at Ω, which arise from the interference between the carrier and sideband components. Keeping only the beat terms between the carrier and sidebands, we find:

$$I(t) \supset \epsilon_\phi \cdot \text{Re}\left[A_+ - A_-\right]\cos(\Omega t) + \epsilon_\phi \cdot \text{Im}\left[A_+ - A_-\right]\sin(\Omega t) \tag{3}$$

where we define:

$$A_\pm = r(\omega_0) r^*(\omega_0 \pm \Omega)$$

4. Demodulation with Arbitrary Phase

The signal is demodulated using a local oscillator $\cos(\Omega t + \phi)$, where ϕ is the demodulation phase. Using trigonometric identities:

$$\cos(\Omega t + \phi) = \cos(\Omega t)\cos\phi - \sin(\Omega t)\sin\phi$$

we multiply Equation (3) and low-pass filter to obtain:

$$\epsilon_{\text{PDH}}(\phi) \propto \epsilon_\phi \left\{\text{Re}[A_+ - A_-]\cos\phi + \text{Im}[A_+ - A_-]\sin\phi\right\} \tag{4}$$

5. Sidebands Far Off-Resonance Approximation

In the standard PDH regime, the modulation frequency is much greater than the cavity linewidth:

$$\Omega \gg \kappa$$

so the sidebands are far off-resonance. This means:

$$r(\omega_0 \pm \Omega) \approx 1 \quad \Rightarrow \quad A_\pm \approx r(\omega_0)$$

and therefore:

$$A_+ - A_- \approx 0$$

However, if we retain the asymmetry between the sidebands (e.g., due to dispersion), or keep the finite detuning contribution, we approximate:

$$A_+ - A_- \approx r(\omega_0)\left[r^*(\omega_0 + \Omega) - r^*(\omega_0 - \Omega)\right] = r(\omega_0)\Delta r^*$$

6. Final Result

Substituting into Equation (4), we obtain:

$$\epsilon_{\text{PDH}}(\phi) \propto \epsilon_\phi \left\{\text{Re}[r(\omega_0)\Delta r^*]\cos\phi + \text{Im}[r(\omega_0)\Delta r^*]\sin\phi\right\} \tag{5}$$

In the limit where $\Delta r^* \to 1$ (normalized, symmetric sidebands), this simplifies to:

$$\boxed{\epsilon_{\text{PDH}}(\omega_0, \phi) \propto \cos\phi \cdot \text{Re}[r(\omega_0)] + \sin\phi \cdot \text{Im}[r(\omega_0)]} \tag{6}$$

7. Interpretation

Equation (6) shows that the demodulated error signal is a linear superposition of the real and imaginary parts of the complex reflection coefficient. The demodulation phase ϕ selects the detected quadrature:

- $\phi = 0$: error signal is proportional to $\mathrm{Re}[r]$ — symmetric around resonance, not suitable for locking.
- $\phi = \pi/2$: error signal is proportional to $\mathrm{Im}[r]$ — antisymmetric, ideal dispersive error signal.
- $\phi \neq 0, \pi/2$: mixes quadratures, possibly introducing offset or distortion.

This derivation makes explicit how the PDH method uses phase-sensitive detection to extract the component of the reflection coefficient that varies linearly with detuning, enabling precise feedback locking of the laser to the cavity resonance.

Pierre-Edouard Jacquet **????? 2025**

Sujet : Progress towards cryogenic squeezed light optomechanics

Résumé : .

Mots clés : Optomecanique, Lumière comprimée, Cavité de grande Finesse, Interferométrie, Bruit thermique, Bruit de grenaille quantique, Resonateur de grand facteur de Qualité, Interféromètres pour la detection d'ondes gravitationnelles, Bruit de pression de radiation quantique

Subject : Optomechanics and squeezed light

Abstract:

Keywords : Optomechanics, Squeezing, High-Finesse cavity, Interferometry, Thermal Noise, Quantum Shot Noise, High-Q Resonator, Gravitational wave Interferometer,Quantum Radiation Pressure Noise